



# Engineering the gain and bandwidth in avalanche photodetectors

CESAR BARTOLO-PEREZ,<sup>1</sup> AHASAN AHAMED,<sup>1</sup> AHMED S. MAYET,<sup>1</sup> AMITA RAWAT,<sup>1</sup> LISA MCPHILLIPS,<sup>1</sup> SOROUSH GHANDIPARSI,<sup>1</sup> JULIEN BEC,<sup>2</sup> GERARD ARIÑO-ESTRADA,<sup>2</sup> SIMON CHERRY,<sup>2</sup> SHIH-YUAN WANG,<sup>3</sup> LAURA MARCU,<sup>2</sup> AND M. SAIF ISLAM<sup>1,\*</sup>

<sup>1</sup>Electrical and Computer Engineering, University of California – Davis, Davis, California 95616, USA

<sup>2</sup>Department of Biomedical Engineering, University of California – Davis, Davis, California 95616, USA

<sup>3</sup>W&WSens Devices, Inc., 4546 El Camino, Suite 215, Los Altos, California 94022, USA

\*sislam@ucdavis.edu

**Abstract:** Avalanche and Single-Photon Avalanche photodetectors (APDs and SPADs) rely on the probability of photogenerated carriers to trigger a multiplication process. Photon penetration depth plays a vital role in this process. In silicon APDs, a significant fraction of the short visible wavelengths is absorbed close to the device surface that is typically highly doped to serve as a contact. Most of the photogenerated carriers in this region can be lost by recombination, get slowly transported by diffusion, or multiplied with high excess noise. On the other hand, the extended penetration depth of near-infrared wavelengths requires thick semiconductors for efficient absorption. This diminishes the speed of the devices due to the long transit time in the thick absorption layer that is required for detecting most of these photons. Here, we demonstrate that it is possible to drive photons to a critical depth in a semiconductor film to maximize their gain-bandwidth performance and increase the absorption efficiency. This approach to engineering the penetration depth for different wavelengths in silicon is enabled by integrating photon-trapping nanoholes on the device surface. The penetration depth of short wavelengths such as 450 nm is increased from 0.25  $\mu\text{m}$  to more than 0.62  $\mu\text{m}$ . On the other hand, for a long-wavelength like 850 nm, the penetration depth is reduced from 18.3  $\mu\text{m}$  to only 2.3  $\mu\text{m}$ , decreasing the device transit time considerably. Such capabilities allow increasing the gain in APDs by almost 400 $\times$  at 450 nm and by almost 9 $\times$  at 850 nm. This engineering of the penetration depth in APDs would enable device designs requiring higher gain-bandwidth in emerging technologies such as Fluorescence Lifetime Microscopy (FLIM), Time-of-Flight Positron Emission Tomography (TOF-PET), quantum communications systems, and 3D imaging systems.

© 2022 Optica Publishing Group under the terms of the [Optica Open Access Publishing Agreement](#)

## 1. Introduction

Avalanche photodetectors such as APDs and SPADs are made of semiconductor materials with an internal gain which yields higher overall signal-to-noise ratios in photoreceiver modules. Enhancing their gain and bandwidth are critical for high-resolution imaging systems required in the area of biophotonics, such as FLIM [1,2] and TOF-PET [3,4], in navigation systems based on LIDAR, and in new optical communications systems such as quantum communications and free-space optical links [5–8]. Photodetectors can generally present high responsivity, but low bandwidth, or vice versa. This is a trade-off known as the gain-bandwidth product (GBP), an important figure of merit for APDs.

The gain in APDs originates from impact ionization, a stochastic process that results in excess noise relative to shot noise, and therefore limits the gain-bandwidth [9]. Different methods have been explored to achieve low noise and gain-bandwidth, such as selecting a semiconductor with

favorable impact ionization coefficients, scaling down the multiplication region to exploit the impact ionization of carriers that become less dependent on the local electric field [10,11], or impact ionization engineering using appropriately designed heterojunctions [9,12,13]. In an APD structure with an N-on-P doping profile, with the multiplication region close to the surface, the avalanche multiplication will be mainly triggered by the holes when short wavelengths illuminate the device since most of the photons will be absorbed close to the surface. As the ionization coefficient for holes is smaller than that for electrons, the total current gain will be lower for short-wavelength than that for longer wavelengths. Thus, two variants of APD devices are commonly fabricated, N-on-P for greater gain and sensitivity at longer wavelengths (enhanced red-NIR sensitivity) [14], and P-on-N for shorter wavelengths (enhanced UV/blue sensitivity) [15]. In silicon, longer wavelengths penetrate deeper into the structure and require the use of longer absorbing layers at the expense of a reduction in bandwidth [14]. One of the key material properties that determine the gain-bandwidth product and the excess noise of APDs is the effective  $k$  ratio of the ionization coefficient of electrons versus holes. Low  $k$  values are desirable for high-performance APDs [16], making silicon an attractive material for APDs due to its low  $k$  value ( $<0.1$ ) that results in a low excess-noise factor,  $F$ . Another key parameter impacting the gain is penetration depth. A penetration depth is a measure of how deep the electromagnetic wave penetrates the material. It is defined as the depth at which the intensity of radiation inside the material falls to  $1/e$  (37%) of its value at the surface. This parameter plays a critical role in APDs by making the gain a function of the incident wavelength [17].

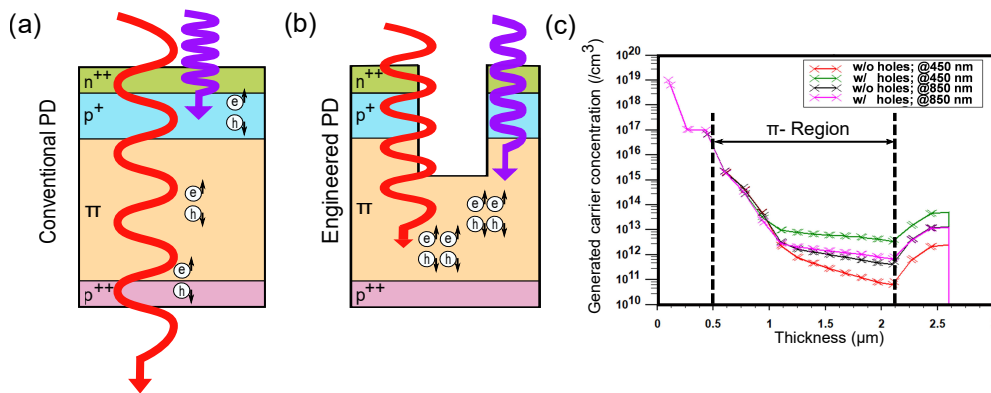


**Fig. 1.** (a) Conventional penetration depth of short and long wavelengths in an avalanche PD structure with separate absorption and multiplication layers. Short wavelengths (such as blue light from 380 nm to 485 nm) are mostly absorbed close to the surface due to their high absorption coefficient. Longer wavelengths (such as red and near-infrared light from 625 nm to 1100 nm) travel deeper into the device. (b) A potential engineered PD with integrated photon trapping nanoholes can modify the penetration depth of the incident light. Shorter wavelengths travel deeper while longer wavelengths can be absorbed at a shorter distance. (c) Generated carrier concentration comparison between w/o holes and w/ holes PD structures both for 450 nm and 850 nm wavelengths.

The implementation of photon trapping nanoholes enhances the absorption of silicon photodetectors at long infrared wavelengths by diffraction of the light in the hole array and generation of laterally propagating waves [18,19]. An increase in speed is also achieved by using a thinner absorbing layer and by reducing the effective area of the device to decrease the capacitance by more than 50% [20]. However, avalanche photodetectors are complex devices that also require a low multiplication of noise while increasing their GBP.

In this work, we propose a method to engineer the gain and bandwidth of avalanche photodiodes by controlling the penetration depth of light in the semiconductor with the implementation of photon trapping nanoholes. We demonstrate the control of the penetration depth of light into silicon APDs which promotes the initialization of impact ionization by electrons and leads to a lower multiplication noise, and a higher gain-bandwidth desired in avalanche-based photodiodes [Fig. 1(a-b)]. We have fabricated Si-photodetectors with photon trapping nanoholes of different profiles that change the penetration depth of 450 nm and 850 nm wavelength light and observed how the gain is impacted in both devices.

## 2. Simulations, design, and fabrication

### 2.1. Optical simulations of photon trapping nanoholes

Optical and electrical simulations of a typical APD silicon photodetector (P-on-N) with implemented nanostructures show the electromagnetic wave interference in presence of photon-trapping structures. To study the impact of photon-trapping structures on generated conducting carriers in presence of illumination, an ATLAS Silvaco TCAD simulation is performed. The presence of photon-trapping structures increases the carrier generation by an order of magnitude for 450 nm as well as 850 nm light wavelengths as shown in Fig. 1(c). Such enhancement in the generated carrier concentration could be attributed to penetration depth modulation for both wavelengths. Due to the diffraction, the penetration depth for lower wavelengths such as 450 nm, increases, and due to the very same diffraction, the penetration depth for higher wavelengths such as 850 nm, decreases—resulting in enhanced absorption in the  $\pi$ -region—causing enhanced carrier generation.

To strengthen our arguments, we have further performed Finite-Difference Time-Domain (FDTD) simulations to study the interaction of the incident electromagnetic wave in silicon with photon-trapping structures. Previously, a Rigorous Coupled-Wave Analysis (RCWA) was performed to study the diffraction of light inside the different layers of a PD with a nanohole array [19]. However, the FDTD analysis determines the power absorption more precisely in different regions of the semiconductor and calculates the penetration depth of the incident light in the engineered device. The light is incident from the top at an angle normal to the surface. Periodic Boundary Conditions (PBC) are applied in the lateral directions and Perfect Matching Layers (PML) are applied in the vertical directions. The total power of the light absorbed is calculated throughout the semiconductors and integration is performed for every 50 nm of depth to calculate the power decay against the distance from the surface. Such a process allows comparing the penetration depth ( $\delta$ ) of the incident light for PDs with different photon-trapping nanoholes ( $\delta_{engineered}$ ) and conventional PDs ( $\delta_{conventional}$ ).

The first set of FDTD simulations is performed to understand the penetration depth and the optical generation of carriers when light with wavelengths of 450 nm and 850 nm are injected into the fabricated devices. The next set of optical simulations is used to calculate the penetration depths generated by varying parameters for holes with depths at a fixed wavelength, and when different wavelengths are incident in the photodetector.

### 2.2. Device design and fabrication

Silicon photodetectors are fabricated with a mesa-type structure, where the doping layers are epitaxially grown as a P-I-N structure with a total thickness of 2.5  $\mu\text{m}$  as shown in Fig. 2(a-b). This structure will favor the enhancement of shorter wavelengths, but a similar approach can be implemented on an N-I-P structure for longer wavelengths. Different nanohole designs are implemented in the silicon photodetectors: inverted pyramid, funnel shape, and cylindrical hole [Fig. 2(c)]. These nanoholes have a diameter ( $d$ ) of 1000 nm and a periodicity ( $p$ ) of 1300 nm. The depths of the cylindrical and funnel-shaped holes were measured to be 2  $\mu\text{m}$  and 2.5  $\mu\text{m}$ ,

respectively, by Scanning Electron Microscopy (SEM). For the inverted pyramid hole, the depth was measured to be  $0.8 \mu\text{m}$ , which is calculated by considering the etching angle in silicon of  $54.7^\circ$  with respect to the surface, created when KOH is used to etch silicon in the  $<100>$  plane.

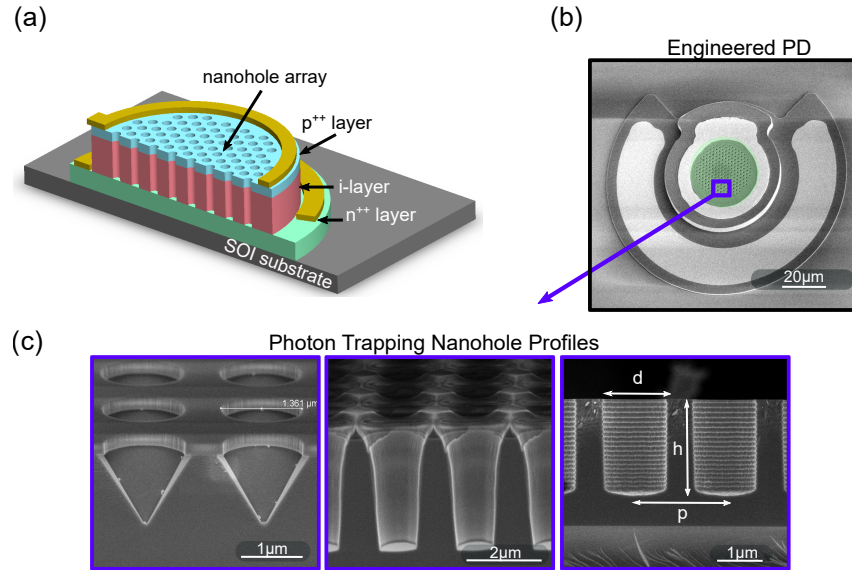


**Fig. 2.** (a) Schematic of engineered PD with photon trapping nanoholes with a PIN structure for proof of concept. (b) SEM of fabricated PD. (c) Different photon trapping nanohole profiles to study the penetration depth and gain.

### 2.3. Characterization of photodetectors

Current-Voltage (I-V) measurements were performed on different fabricated devices under dark conditions and under optical illumination at 450 nm and 850 nm wavelengths with a total power of  $1 \mu\text{W}$  for each. This light was delivered to the PD through an optical fiber with an incident angle normal to the surface. A fiber splitter was used to tap 10% of the light for continuous monitoring of the incident light power. From the I-V measurements, the multiplication gain in the engineered and the conventional PD was calculated as  $M = [I_{photo(V)} - I_{dark(V)}]/[I_{photo(V_{ref})} - I_{dark(V_{ref})}]$ , where  $V_{ref}$  was taken at 10 V. Multiple PDs with the same profile are characterized on different wafers to evaluate the stochasticity of the APD behavior showing a variation of up to  $\pm 9.6\%$  in the measured gain.

## 3. Results and discussion

### 3.1. Multiplication gain for 450 nm and 850 nm wavelength

At an input wavelength of 850 nm, our devices exhibit a gain factor increase from  $M = 97.9$ , in the conventional PD, to a maximum of  $M = 893$  for the engineered PD with the inverted pyramid hole profile, followed by the funnel ( $M = 770.3$ ) and the cylindrical hole profile ( $M = 515.2$ ) [Fig. 3(e)]. The amount of light absorbed with respect to the thickness of the PD is presented in Fig. 3(b). When overlapping the schematic of the doping profile of Fig. 3(c), it is observed that more light is absorbed in the i-layer. The FDTD simulations showed that the penetration depth ( $\delta$ ) of the 850 nm wavelength-light in the inverted pyramid design was reduced from  $\delta_{conventional} = 18.4 \mu\text{m}$  to  $\delta_{engineered} = 2.3 \mu\text{m}$  [Fig. 3(d)]. The implementation of this nanohole profile also reduces the reflection from 32% to 17% and increases the absorption in the  $2.5 \mu\text{m}$ -thickness devices from 8%

to 61% [Fig. 3(a)]. This nanohole design exhibited higher absorption, shorter penetration depth, and greater maximum gain. The control of the penetration depth, the reduction of reflection, and the increase of absorption, all collectively increase the gain and allow the fabrication of Si PDs with thinner absorbing layers for high bandwidth operation.

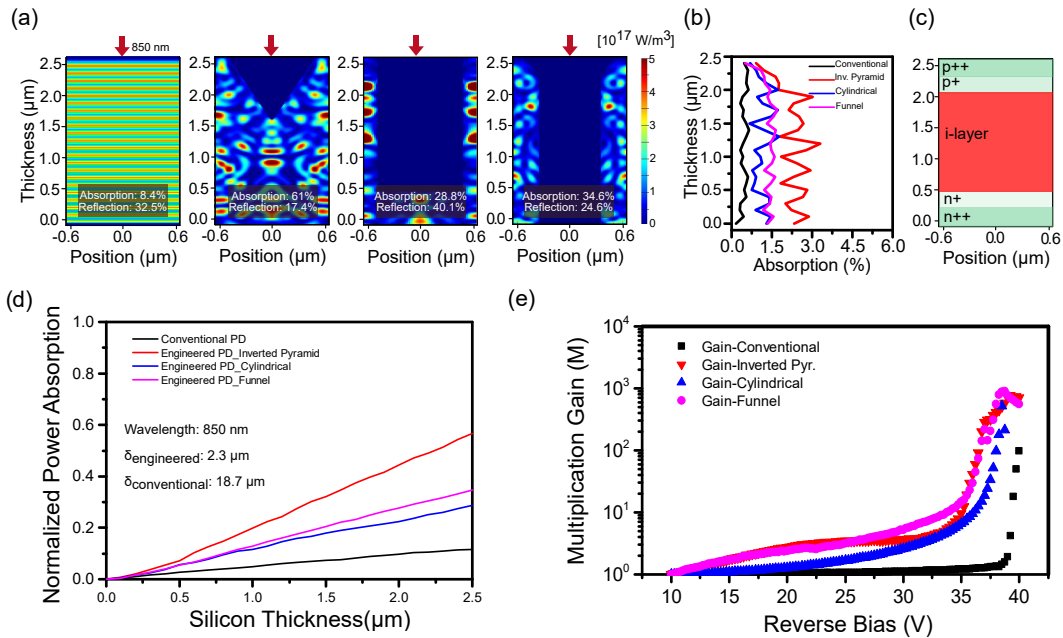


**Fig. 3.** (a) Power absorption of light at 850 nm wavelength in the conventional and engineered PDs with diverse nanohole profiles, simulated by FDTD. (b) Percentage of absorbed light with respect to the depth. (c) Schematic of the doping profile of the fabricated PD. (d) Comparison of the penetration depth between conventional ( $\delta_{\text{conventional}}$ ) and engineered ( $\delta_{\text{engineered}}$ ) APDs for 850 nm wavelength.  $\delta$  is reduced from 18.7  $\mu\text{m}$  to 2.3  $\mu\text{m}$ . (e) Experimental multiplication gain measurements: comparison between conventional PD and engineered PDs with different nanohole profiles.

For an input wavelength of 450 nm, our conventional Si PDs exhibited a maximum multiplication gain of 11.9. On the other hand, our engineered PDs present a gain of  $M = 4707.9$  for the cylindrical hole, followed by the funnel-shaped nanohole ( $M = 3925$ ) and the inverted pyramid ( $M = 3508.3$ ) [Fig. 4(d)]. FDTD simulations of the PD with cylindrical holes show that the 450 nm-wavelength light penetrates deeper into the semiconductor [Fig. 4(b)], moving from a penetration depth of 0.25  $\mu\text{m}$  in the conventional PD to a maximum of 0.75  $\mu\text{m}$  in the engineered PD with cylindrical nanohole [Fig. 4(c)]. Contrary to the 850 nm wavelength case, at 450 nm the gain increases in devices with nanohole designs that allow a deeper penetration depth. In addition to the gain enhancement, the implementation of nanoholes increases the absorption in silicon from 60% to 83.5%, and a reduction in reflection from 40% to 14% [Fig. 4(a)]. Figure 4(e)-(g) shows the current-voltage characteristics under dark conditions and illumination for a conventional PD (e) and for engineered PD-Cylindrical with an input wavelength of 450 nm (f), and 850 nm (g). Lastly, Table 1 summarizes the obtained results with respect to the penetration depth, gain and External Quantum Efficiency (EQE) obtained in our fabricated devices at 450 nm and 850 nm wavelength light.

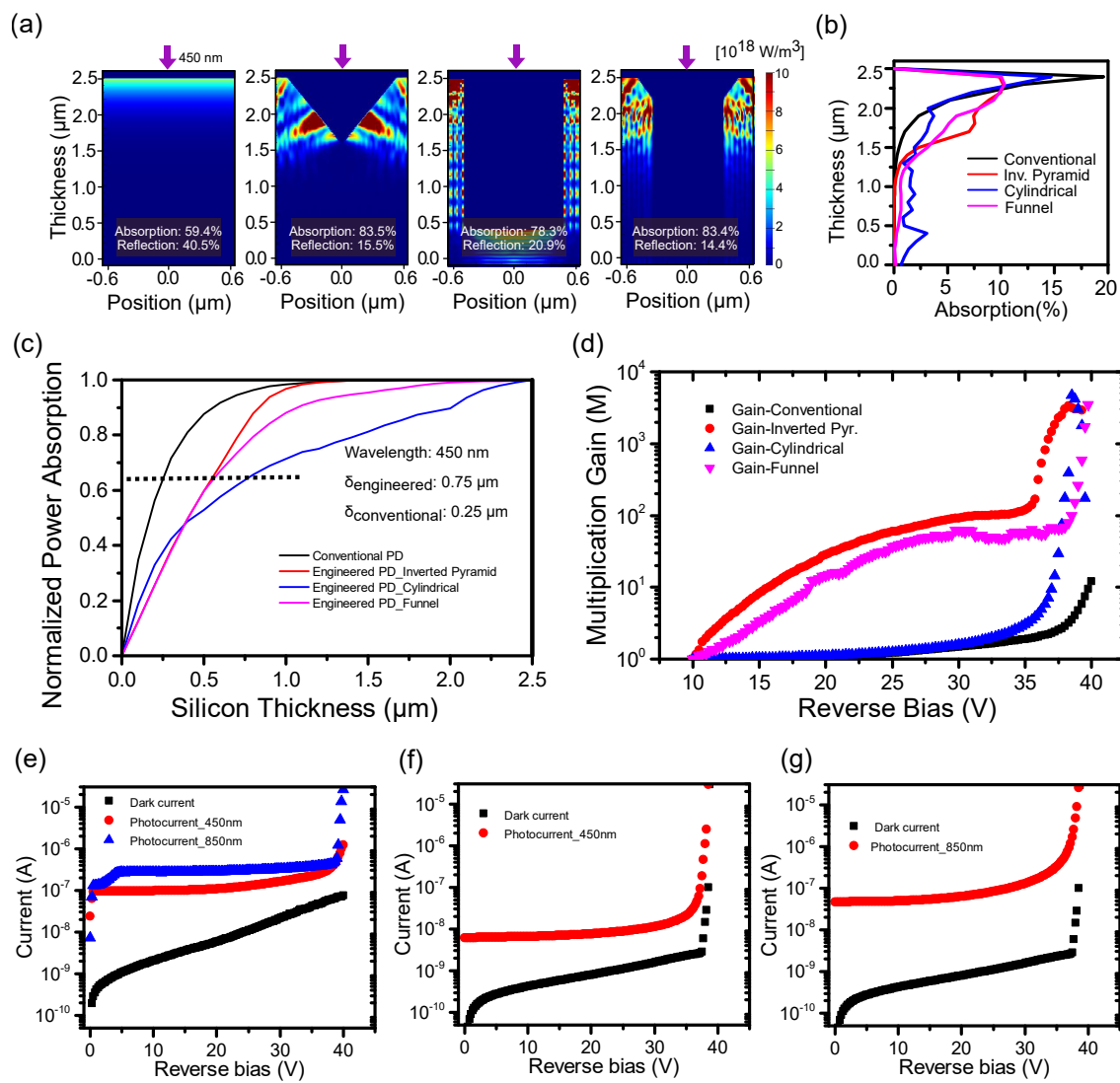


**Fig. 4.** (a) Power absorption of light at 450 nm wavelengths in the conventional and engineered PDs with different nanohole profiles, simulated by FDTD. (b) Percentage of absorbed light with respect to the depth. (c) Comparison of penetration depth between conventional ( $\delta_{\text{conventional}}$ ) and engineered ( $\delta_{\text{engineered}}$ ) APD.  $\delta$  increased from 0.25  $\mu\text{m}$  to 0.75  $\mu\text{m}$ . (d) Experimental multiplication gain measurements comparing conventional PD and engineered PDs. The gain increases by nearly a factor of four hundred, from 11.9 to more than 4000. (e-f) Current-Voltage under dark conditions and illumination for a conventional PD (e), and Engineered PD-Cylindrical with an input light wavelength of 450 nm (f), and 850 nm (g).

### 3.2. Engineering of penetration depth at 450 nm wavelength

As shown in the previous section, engineering of the penetration depth allows the modification of the gain obtained in an APD. Furthermore, the bandwidth of photodetectors is enhanced by reducing the transit time of the photogenerated carriers. A series of simulations have been performed in Si PDs with absorbing layers of only 1.2  $\mu\text{m}$ -thickness to understand the influence

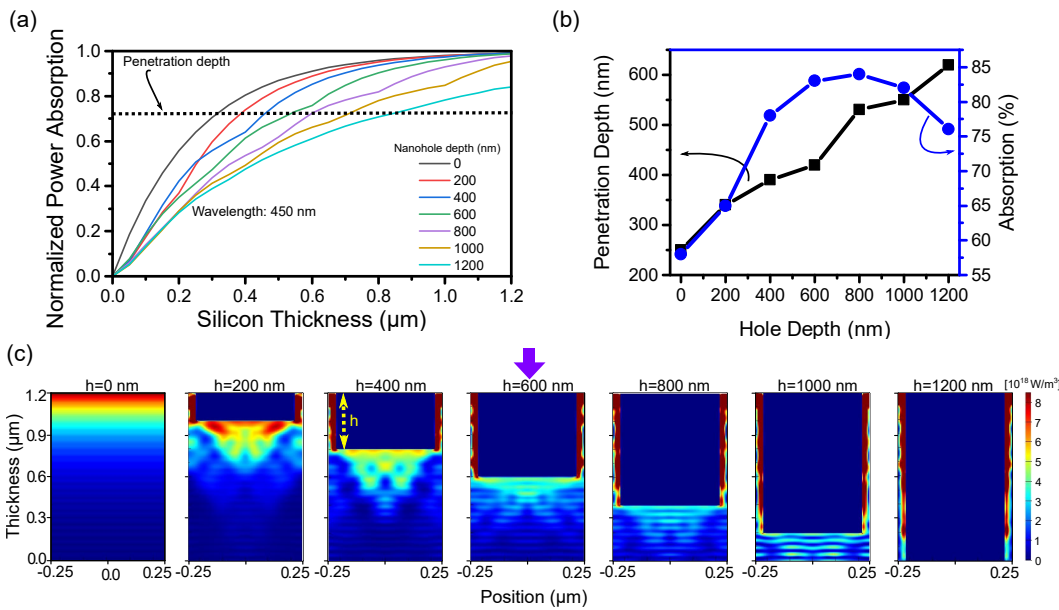


**Fig. 5.** (a) Penetration depth of 450 nm wavelength light in varying photon-trapping nanohole depths. The penetration depth increases with the depth of the hole from 250 nm to 620 nm. (b) Absorption and penetration depth for different hole depths at 450 nm wavelength. A maximum of 84% of absorption can be obtained at 800 nm nanohole depth. (c) Optical absorption profile obtained by FDTD for an incident light of 450 nm.

**Table 1. Penetration depth, multiplication gain, and EQE in silicon photodetectors with different nanohole profiles. The gain in APDs with photon-trapping holes is measured to be almost 400-fold higher at 450 nm and almost 9-fold higher at 850 nm**

	Wavelength (nm)	Conventional	Inverted Pyramid	Cylindrical	Funnel
Penetration depth ( $\mu\text{m}$ )	450	0.25	0.55	0.75	0.61
	850	18.7	2.3	>2.5	>2.5
Multiplication Gain (M)	450	11.9	3508.3	4707.9	3925.8
	850	97.9	893.8	515.8	770.3
External Quantum Efficiency (%) for $M = 1$	450	54	82	74	79
	850	14	56	39	42

of the nanohole depth and incident light wavelengths, in the penetration depth. By varying the nanohole depth from 0 nm (conventional PD) to 1200 nm, the impact of this parameter on penetration depth could be studied. For this study, an incident wavelength of 450 nm illuminated the PD, with an incident angle normal to the surface of the device. Cylindrical holes, with 480 nm diameter (d) and 500 nm period (p) are used in this study. The power absorption with respect to depth is calculated for each 50 nm segment along with the depth. Figure 5(a) shows that the penetration depth increases from 0.25  $\mu\text{m}$  in the conventional PD to a maximum of 0.63  $\mu\text{m}$  when cylindrical holes are etched with 1200 nm depth. However, etching the nanoholes can also reduce the absorption and increase the transmission of the light, making it necessary to optimize the etching depth. Figure 5(b) shows that the maximum absorption and penetration depth for this design is obtained with a nanohole depth of 800 nm where 84% of the light is absorbed and the penetration depth is 0.54  $\mu\text{m}$ .

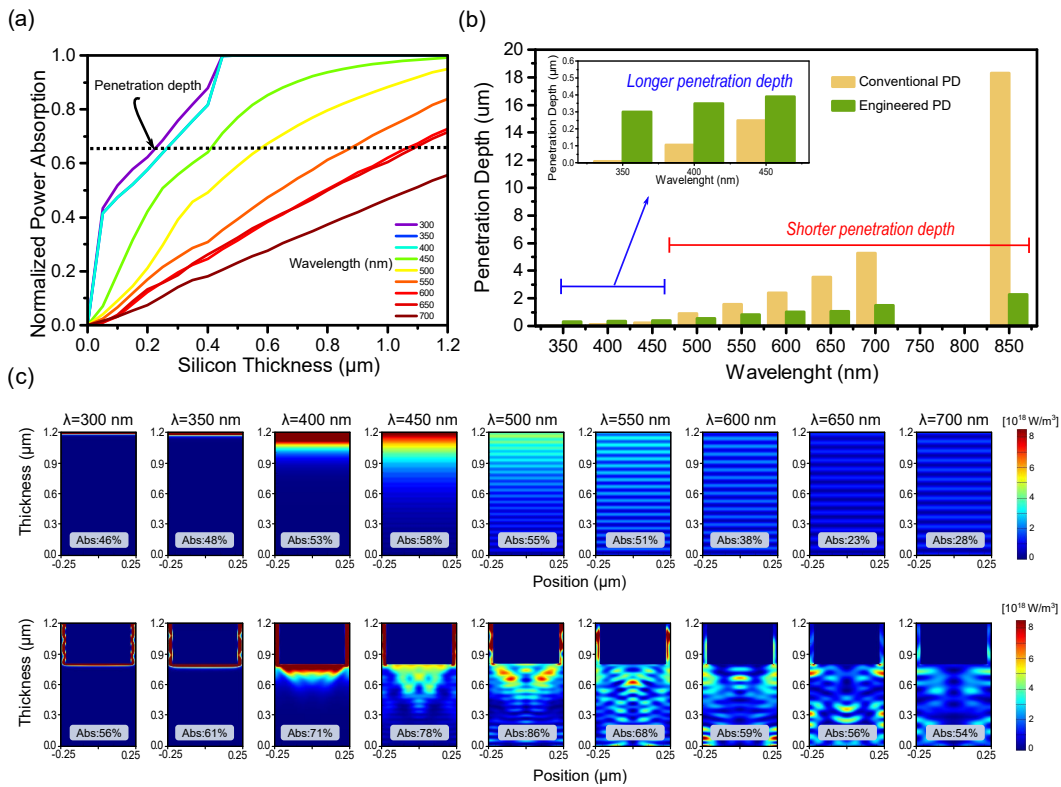


**Fig. 6.** (a) Penetration depth engineered on silicon for incident light wavelengths between 300 nm to 700 nm. (b) Comparison of penetration depth between conventional and engineered PDs. At wavelengths below 450 nm, the penetration depth is dramatically increased, reducing the loss of carriers by recombination, slow diffusion transport, and high excess noise multiplication. Above 500 nm wavelength, the penetration depth is reduced by more than 50%. At 850 nm the penetration depth is reduced from 18.3  $\mu\text{m}$  to only 2.3  $\mu\text{m}$ , an 87% reduction in the depth. (c) The power distribution of incident light at different wavelengths on conventional and photon-trapping photodiodes for nanoholes depth of 400 nm, a diameter of 480 nm, and a period of 500 nm.

At 450 nm wavelength, silicon exhibits a high absorption coefficient but also reflects 40% of the incident light. With the integrated nanohole approach, the reflection is reduced to approximately 10%. Figure 5(c) shows the power distribution of the 450 nm wavelength light in the engineered PDs with different nanohole depths.

### 3.3. Engineering the photon penetration depth for visible and NIR wavelengths

A broad range of applications works in the visible wavelengths, making it important to study the change in penetration depth inside of silicon for different input wavelengths from 300 nm to 850 nm when implementing the nanoholes in silicon. We fixed the nanohole depth at 400 nm and kept the diameter and the period unchanged (480 nm diameter and 500 nm period).

Figure 6(a) shows the normalized power absorption for different wavelengths in the engineered PD with respect to its thickness. These curves are used to calculate their respective penetration depth. Figure 6(b) compares the penetration depth of conventional devices and the engineered PDs. For wavelengths below 450 nm, our simulations show that a greater penetration depth is achieved [Fig. 6(b), inset]. On the other hand, from 500 nm to 850 nm wavelength, the increase in

absorption achieved with nanoholes decreases the penetration depth to a range between 0.55  $\mu\text{m}$  to 2.3  $\mu\text{m}$ . Shorter wavelengths (such as 450 nm) are observed to penetrate deeper into silicon. On the other hand, photons with longer wavelengths (such as 850 nm) are forced to propagate to shallower depths. Figure 6(c) represents the different distribution of light absorbed in the conventional silicon PD and the engineered PD, for 450 nm wavelengths.

#### 4. Conclusions

We have demonstrated that it is possible to guide photons to a critical depth in a semiconductor and maximize the gain-bandwidth performance and absorption efficiency in avalanche-based photodetectors by integrating photon-trapping nanoholes with different profiles and depths on the device surface. Such nanoholes allow for the engineering of the penetration depth for different wavelengths on silicon. A longer penetration depth for short wavelengths such as 450 nm can reduce the absorption close to the surface of the device, where carriers can be lost by recombination or slowly transported by diffusion. On the other hand, the penetration depth for the long wavelengths such as 850 nm is reduced from 18.3  $\mu\text{m}$  to only 2.3  $\mu\text{m}$ . Such reduction in penetration depth allows decreasing the device transit time with a direct impact on the bandwidth of the devices. These results allow increasing the gain in APDs by 400 times at 450 nm and by more than 9 times at 850 nm. The engineering of the penetration depth in APDs and SPADs allows designing devices with higher gain-bandwidth required in a myriad of emerging applications including biomedical imaging systems such as FLIM and TOF-PET, quantum communications systems, and 3D imaging systems.

**Funding.** UC Davis College of Engineering (Dean's Collaborative Research Award (DECOR)); National Council of Science and Technology (CONACYT, Mexico, UC-MEXUS); National Institute of Biomedical Imaging and Bioengineering (R21 EB028398); S. P. Wang and S. Y. Wang Partnership.

**Acknowledgments.** Cesar Bartolo-Perez acknowledges the National Council of Science and Technology (CONACYT) and UC-MEXUS for the Doctoral fellowship. Part of this study was carried out at the UC Davis Center for Nano and Micro Manufacturing (CNM2).

**Disclosures.** The authors declare no conflicts of interest

**Data availability.** Data underlying the results presented in this paper are not publicly available at this time but may be obtained from the authors upon reasonable request.

#### References

1. X. Zhou, J. Bec, D. Yankelevich, and L. Marcu, "Multispectral fluorescence lifetime imaging device with a silicon avalanche photodetector," *Opt. Express* **29**(13), 20105–20120 (2021).
2. J. Bec, J. E. Phipps, D. Gorpas, D. Ma, H. Fatakdawala, K. B. Margulies, J. A. Southard, and L. Marcu, "In vivo label-free structural and biochemical imaging of coronary arteries using an integrated ultrasound and multispectral fluorescence lifetime catheter system," *Sci. Rep.* **7**(1), 8960 (2017).
3. C. Bruschini, H. Homulle, I. M. Antolovic, S. Burri, and E. Charbon, "Single-photon avalanche diode imagers in biophotonics: review and outlook," *Light: Sci. Appl.* **8**(1), 87 (2019).
4. C. Bartolo-Perez, S. Ghandiparsi, A. Mayet, H. Cansizoglu, Y. Gao, W. Qarony, A. Ahamed, S.-Y. Wang, S. Cherry, M. S. Islam, and G. Ariño-Estrada, "Avalanche Photodetectors with Photon Trapping Structures for Biomedical Imaging Applications," in 2021,
5. S. Huang and M. Safari, "Hybrid SPAD/PD Receiver for Reliable Free-Space Optical Communication," *IEEE Open J. Commun. Soc.* **1**, 1364–1373 (2020).
6. M. M. Hossain, S. Ray, J. S. Cheong, L. Qiao, A. N. A. P. Baharuddin, M. M. Hella, J. P. R. David, and M. M. Hayat, "Low-Noise Speed-Optimized Large Area CMOS Avalanche Photodetector for Visible Light Communication," *J. Lightwave Technol.* **35**(11), 2315–2324 (2017).
7. L. Zhang, D. Chitnis, H. Chun, S. Rajbhandari, G. Faulkner, D. O'Brien, and S. Collins, "A Comparison of APD- and SPAD-Based Receivers for Visible Light Communications," *J. Lightwave Technol.* **36**(12), 2435–2442 (2018).
8. L. Zhang, H. Chun, Z. Ahmed, G. Faulkner, D. O'Brien, and S. Collins, "The Future Prospects for SiPM-Based Receivers for Visible Light Communications," *J. Lightwave Technol.* **37**(17), 4367–4374 (2019).
9. J. C. Campbell, "Recent Advances in Avalanche Photodiodes," *J. Lightwave Technol.* **34**(2), 278–285 (2016).
10. P. Yuan, C. C. Hansing, K. A. Anselm, C. V. Lenox, H. Nie, A. L. Holmes, B. G. Streetman, and J. C. Campbell, "Impact ionization characteristics of III-V semiconductors for a wide range of multiplication region thicknesses," *IEEE J. Quantum Electron.* **36**(2), 198–204 (2000).

11. R. J. McIntyre, "A new look at impact ionization-Part I: A theory of gain, noise, breakdown probability, and frequency response," *IEEE Trans. Electron Devices* **46**(8), 1623–1631 (1999).
12. S. D. March, A. H. Jones, J. C. Campbell, and S. R. Bank, "Multistep staircase avalanche photodiodes with extremely low noise and deterministic amplification," *Nat. Photonics* **15**(6), 468–474 (2021).
13. J. C. Campbell, "Evolution of Low-Noise Avalanche Photodetectors," *IEEE J. Sel. Top. Quantum Electron.* **28**(2), 1–11 (2022).
14. A. Gulinatti, I. Rech, F. Panzeri, C. Cammi, P. Maccagnani, M. Ghioni, and S. Cova, "New silicon SPAD technology for enhanced red-sensitivity, high-resolution timing and system integration," *J. Mod. Opt.* **59**(17), 1489–1499 (2012).
15. F. Acerbi, A. Ferri, G. Zappala, G. Paternoster, A. Picciotto, A. Gola, N. Zorzi, and C. Piemonte, "NUV Silicon Photomultipliers With High Detection Efficiency and Reduced Delayed Correlated-Noise," *IEEE Trans. Nucl. Sci.* **62**(3), 1318–1325 (2015).
16. Y. Kang, H.-D. Liu, M. Morse, M. J. Paniccia, M. Zadka, S. Litski, G. Sarid, A. Pauchard, Y.-H. Kuo, H.-W. Chen, W. S. Zaoui, J. E. Bowers, A. Beling, D. C. McIntosh, X. Zheng, and J. C. Campbell, "Monolithic germanium/silicon avalanche photodiodes with 340 GHz gain-bandwidth product," *Nat. Photonics* **3**(1), 59–63 (2009).
17. P. Webb and M. Rj, "Properties of Avalanche Photodetectors," *RCA review* **35**, 234–278 (1974).
18. Y. Gao, H. Cansizoglu, K. G. Polat, S. Ghandiparsi, A. Kaya, H. H. Mamtaz, A. S. Mayet, Y. Wang, X. Zhang, T. Yamada, E. P. Devine, A. F. Elrefaei, S.-Y. Wang, and M. S. Islam, "Photon-trapping microstructures enable high-speed high-efficiency silicon photodiodes," *Nature Photon* **11**(5), 301–308 (2017).
19. G. Jun, C. Hilal, B.-P. Cesar, G. Soroush, S. M. Ahmed, R.-G. Hossein, G. Yang, W. Jun, Y. Toshishige, D. Ekaterina Ponizovskaya, F. E. Aly, W. Shih-Yuan, and M. S. Islam, "Rigorous coupled-wave analysis of absorption enhancement in vertically illuminated silicon photodiodes with photon-trapping hole arrays," *Nanophotonics* **8**(10), 1747–1756 (2019).
20. C. Bartolo-Perez, W. Qarony, S. Ghandiparsi, A. S. Mayet, A. Ahamed, H. Cansizoglu, Y. Gao, E. Ponizovskaya Devine, T. Yamada, A. F. Elrefaei, S.-Y. Wang, and M. S. Islam, "Maximizing Absorption in Photon-Trapping Ultrafast Silicon Photodetectors," *Adv Photo Res* **2**(6), 2000190 (2021).